Multiobjective Optimization of OFDM Radar Waveform for Target Detection

Satyabrata Sen, *Member, IEEE*, Gongguo Tang, *Member, IEEE*, and Arye Nehorai, *Fellow, IEEE*

***Abstract*—We propose a multiobjective optimization (MOO) technique to design an orthogonal-frequency-division multiplexing (OFDM) radar signal for detecting a moving target in the presence of multipath reflections. We employ an OFDM signal to increase the frequency diversity of the system, as different scattering centers of a target resonate variably at different frequencies. Moreover, the multipath propagation increases the spatial diversity by providing extra "looks" at the target. First, we develop a parametric OFDM radar model by reformulating the target-detection problem as the task of sparse-signal spectrum estimation. At a particular range cell, we exploit the sparsity of multiple paths and the knowledge of the environment to estimate the paths along which the target responses are received. Then, to estimate the sparse vector, we employ a collection of multiple small Dantzig selectors (DS) that utilizes more prior structures of the sparse vector. We use the ℓ_1-constrained minimal singular value (ℓ_1-CMSV) of the measurement matrix to analytically evaluate the reconstruction performance and demonstrate that our decomposed DS performs better than the standard DS. In addition, we propose a constrained MOO-based algorithm to optimally design the spectral parameters of the OFDM waveform for the next coherent processing interval by simultaneously optimizing two objective functions: minimizing the upper bound on the estimation error to improve the efficiency of sparse-recovery and maximizing the squared Mahalanobis-distance to increase the performance of the underlying detection problem. We provide a few numerical examples to illustrate the performance characteristics of the sparse recovery and demonstrate the achieved performance improvement due to adaptive OFDM waveform design.**

***Index Terms*—Adaptive waveform design, multiobjective optimization, OFDM radar, Pareto-optimal solution, target detection.**

I. Introduction

THE problems of detection and tracking of targets in the presence of multipath, particularly in urban environments, are becoming increasingly relevant and challenging to radar technologies. In [1] and [2], we showed that the target-detection capability can be significantly improved by exploiting multiple Doppler shifts corresponding to the projections of the target velocity on each of the multipath components. Furthermore, the multipath propagations increase the spatial diversity of the radar system by illuminating the target from different incident angles, thus enabling target detection and tracking even beyond the line-of-sight (LOS) [3], [4]. Other areas of application in which multipath effects are of primary interest are in low-angle tracking (sea-skimmers) [5]–[8], height finding [9], [10], radar-aided navigation and landing systems [11], and shallow-water sonar operations [12], [13].

To resolve and exploit the multipath components it is common to use short pulse, multicarrier wideband radar signals. We consider the orthogonal-frequency-division multiplexing (OFDM) signalling scheme [14], [15], which is one way to use several subcarriers simultaneously. The use of an OFDM signal mitigates possible fading, resolves multipath reflections, and provides additional frequency diversity as different scattering centers of a target resonate at different frequencies. Although OFDM has been elaborately studied and commercialized in the digital communication field [16], it has not been studied so widely by the radar community, apart from a few recent efforts [17]–[19].

In this work, we consider a target-detection problem in multipath scenarios from a different perspective. We observe that the radar receives the target information through a LOS, several reflected paths, or both. Therefore, using our knowledge of the geometry, we can determine all the possible paths, be they LOS or reflected, and the associated target locations corresponding to a particular range cell. Then, considering the presence of a single target, we can apply any sparse-signal recovery algorithm [20]–[22] to determine the paths along which the target response is received. Thus, we transform the target-detection problem into the task of estimating the spectrum of a sparse signal.

First, we develop a parametric OFDM measurement model for a particular range cell, to detect a far-field point target moving in a multipath-rich environment. For simplicity, we consider only first-order (or single bounce) specularly reflected multipath signals. Then, we convert the model to a sparse model that accounts for the target returns over all possible signal paths and target velocities. The nonzero components of the sparse vector in our model correspond to the scattering coefficients of the target at different OFDM subcarriers. We assume that the clutter and measurement noise are temporally white.

To estimate the sparse vector, we propose a sparse-recovery algorithm based on the Dantzig selector (DS) approach [22]. The DS approach belongs to the class of convex relaxation methods in which the ℓ_0 norm is replaced by the ℓ_1 norm that remains a measure of sparsity while being a convex function.

Manuscript received July 29, 2010; revised October 12, 2010; accepted October 12, 2010. Date of publication October 28, 2010; date of current version January 12, 2011. The associate editor coordinating the review of this manuscript and approving it for publication was Prof. Xiang-Gen Xia. This work was supported by the Department of Defense under the Air Force Office of Scientific Research MURI Grant FA9550-05-1-0443 and ONR Grant N000140810849.

The authors are with the Department of Electrical and Systems Engineering, Washington University in St. Louis, St. Louis, MO 63130 USA (e-mail: ssen3@ese.wustl.edu; gt2@ese.wustl.edu; nehorai@ese.wustl.edu).

Color versions of one or more of the figures in this paper are available online at http://ieeexplore.ieee.org.

Digital Object Identifier 10.1109/TSP.2010.2089628

Other examples of convex relaxation methods include the basis pursuit [20] and LASSO estimator [23]. However, instead of using the standard DS, in this work we employ a collection of multiple small DS to exploit more prior structures of the sparse vector. Furthermore, we analytically evaluate the performance characteristics and show that our decomposed DS has advantages over the standard DS both in terms of computation and performance. To analyze the reconstruction performance, we consider the ℓ_1-constrained minimal singular value (ℓ_1-CMSV) of the measurement matrix [24]. Compared with the traditional restricted isometry constant (RIC) [25], [26], which is extremely difficult to compute for an arbitrarily given matrix, the ℓ_1-CMSV is an easily computable measure and provides more intuition on the stability of sparse-signal recovery. More importantly, in [24] we already designed several algorithms to compute the ℓ_1-CMSV of any given measurement matrix.

Next, we propose a criterion to optimally design the spectral parameters of the transmitting OFDM waveform for the next coherent processing interval, based on the multiobjective optimization (MOO) approach [27]–[30]. We observe that if the signal parameters are designed to minimize the upper bound on the sparse-estimation error, then the resultant waveform depends solely on the properties of the measurement matrix. However, to achieve a better performance it is also essential that the signal parameters are adaptive to the operational scenario involving dynamic target states and nonstationary environmental conditions. Hence, in addition to minimizing the upper bound on the estimation error, we propose maximizing another utility function based on the squared Mahalanobis-distance [31], [32], one that depends on the target and noise parameters. Based on these arguments, we develop a constrained MOO problem to simultaneously optimize two objective functions: to minimize the upper bound on the estimation error to improve the efficiency of sparse-recovery and to maximize the squared Mahalanobis-distance to increase the performance of the underlying detection problem.

Often, a MOO problem does not have a single optimal solution but rather a set of solutions known as Pareto-optimal solutions [27]. This type of optimality was originally introduced by Edgeworth in 1881 [33] and later generalized by Pareto in 1896 [34]. All the solutions residing on the Pareto-front are superior to other solutions in the search space when all objectives are considered. The idea of finding as many Pareto-optimal solutions as possible motivates the use of evolutionary algorithms (EAs) that generate several solutions in a single run. Following the same motivation, we apply the well-known nondominated sorting genetic algorithm II (NSGA-II) [35] to solve our MOO problem. Previous work in the application of multiobjective evolutionary algorithms (MOEAs) for radar system design includes [36]–[40] and the references therein.

To illustrate the sparse-estimation performance for a target-detection problem and to demonstrate the performance improvement due to the adaptive OFDM waveform design, we present several numerical examples. We evaluate the performance characteristics in terms of the normalized root mean squared error (RMSE) and empirical receiver operating characteristic (ROC). We show that the decomposed DS performs better than the standard DS and requires much less computation time. From the results of the adaptive design, we observe that the solution based on the minimization of the upper bound on the sparse-estimation error depends only on the properties of the measurement matrix, whereas the solutions based on the maximization of the squared Mahalanobis-distance and optimization of the MOO problem depend on the target and noise parameters as well. However, the maximization of the squared Mahalanobis-distance provides an adaptive waveform with all the signal energy transmitted over a single subcarrier that has the strongest target response, thus loosing the frequency diversity of the system. The solution of the MOO-based adaptive design in general produces the best performance. Assuming that the noise powers over different subcarriers are the same, we infer that the solution of the MOO distributes the energy of the optimal waveform across different subcarriers in proportion to the distribution of the target energy; i.e., it puts more signal energy to that particular subcarrier in which the target response is stronger.

The rest of the paper is organized as follows. In Section II, we first present a parametric OFDM radar measurement model and then convert it to a sparse model. Then, in Section III, we present the sparse-recovery algorithm and analytically evaluate its performance characteristics. In Section IV, we propose the adaptive OFDM waveform design algorithm based on the MOO approach. Numerical examples and conclusions are presented in Sections V and VI, respectively.

Notations

We present here some notational conventions that will be used throughout this paper. We use math italic for scalers, lowercase bold for vectors, and uppercase bold for matrices. For a matrix $\boldsymbol{A} \in \mathbb{C}^{k\times m}$, $\boldsymbol{A}^T, \boldsymbol{A}^H, \mathrm{tr}\{\boldsymbol{A}\}$, and $\mathrm{vec}(\boldsymbol{A})$ denote the transpose, conjugate-transpose, trace, and vec-operation of $\boldsymbol{A}$, respectively. $\boldsymbol{I}_k$ represents an identity matrix of dimension k. $\mathrm{diag}(\cdots)$ forms a square matrix with nonzero entries only on the main diagonal. $\mathrm{Re}\{\cdot\}$ and $\mathrm{Im}\{\cdot\}$ are the real and imaginary parts of a complex quantity. Among different types of vector norms, we consider $||\cdot||_1, ||\cdot||_2$, and $||\cdot||_\infty$ (which is the maximum of the absolute values). We denote the number of nonzero components in a vector by $||\cdot||_0$. Additionally, $\langle,\rangle, \otimes$, and $\odot$ are the inner-product, Kronecker product, and element-wise Hadamard product operators, respectively.

II. Problem Description and Modeling

Fig. 1 presents a schematic representation of the problem scenario. We consider a far-field point target in a multipath-rich environment, moving with a constant relative velocity $\boldsymbol{v}$ with respect to the radar. At the operating frequency we assume that the reflecting surfaces produce only specular reflections of the radar signal, and for simplicity we consider only the first-order reflections. We further assume that the radar has complete knowledge of the environment under surveillance. This assumption implies that for a particular range cell (shown as the curved line in Fig. 1) the radar knows all the possible paths, be they LOS or reflected. Now, any target (e.g., Target B) or any image of a target (e.g., Target A or C) residing on the constant-range curved line has the same roundtrip delay and produces returns in the same range cell. Our goal here is to decide whether a target is present (out of

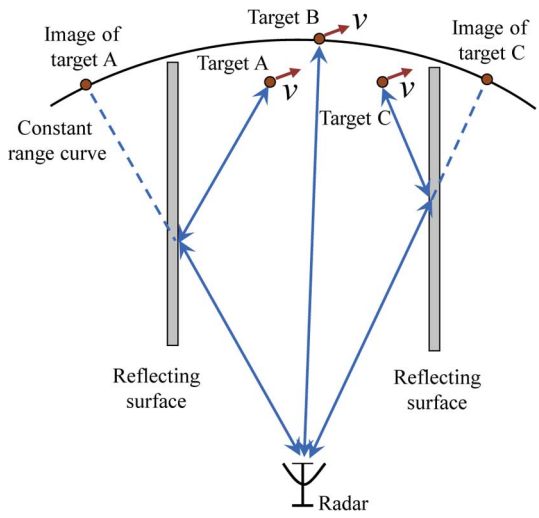

Fig. 1. A schematic representation of the multipath scenario.

all possible paths) at the range cell under test and to determine the corresponding location of the target by using knowledge of the environment.

In the following, we first develop a parametric measurement model by reformulating the target-detection problem as a sparse-estimation method. Then, we discuss our statistical assumptions on the clutter and noise.

A. OFDM Measurement Model

We consider an OFDM signalling system [15] with L active subcarriers, a bandwidth of B Hz, and pulse duration of T seconds. Let $\boldsymbol{a} = [a_0, a_1, \ldots, a_{L-1}]^T$ represent the complex weights transmitted over the L subcarriers, and satisfying $\sum_{l=0}^{L-1} |a_l|^2 = 1$. Then, the complex envelope of the transmitted signal can be represented as

$$s(t) = \sum_{l=0}^{L-1} a_l e^{j2\pi l \Delta f t} \tag{1}$$

where $\Delta f = B/(L+1) = 1/T$ denotes the subcarrier spacing. Let f_c be the carrier frequency of operation; then the transmitted signal is given by

$$\tilde{s}(t) = 2\mathrm{Re}\left\{\sum_{l=0}^{L-1} a_l e^{j2\pi f_l t}\right\} \tag{2}$$

where $f_l = f_c + l\Delta f$ represents the lth subcarrier frequency. Interchanging the real and summation operators, we can rewrite (2) as

$$\tilde{s}(t) = \sum_{l=0}^{L-1} \tilde{s}_l(t) \tag{3}$$

where

$$\tilde{s}_l(t) = 2\mathrm{Re}\{a_l e^{j2\pi f_l t}\} \tag{4}$$

represents the transmitted signal at the lth subcarrier only.

Then, corresponding to a specific range cell (denoted by the roundtrip delay τ), the received signal along the pth path due to only the lth subcarrier can be written as

$$\tilde{y}_l(t) = x_{lp}\tilde{s}_l((1+\beta_p)(t-\tau)) + \tilde{e}_l(t) \tag{5}$$

where x_{lp} is a complex quantity representing the scattering coefficient of the target along the lth subchannel and pth path; $\beta_p = 2\langle \boldsymbol{v}, \boldsymbol{u}_p \rangle / c$ is the relative Doppler shift along the pth path; $\boldsymbol{u}_p$ represents the direction-of-arrival (DOA) unit-vector of the pth path; c is the speed of propagation; and $\tilde{e}_l(t)$ represents the clutter and measurement noise along the lth subchannel. Therefore, the signal received along the pth path due to an L-carrier OFDM signal is given by

$$\begin{aligned}\tilde{y}(t) &= \sum_{l=0}^{L-1} \tilde{y}_l(t) \\ &= 2\mathrm{Re}\left\{\sum_{l=0}^{L-1} a_l x_{lp} e^{j2\pi f_l(1+\beta_p)(t-\tau)}\right\} + \tilde{e}(t), \\ &= 2\mathrm{Re}\left\{\sum_{l=0}^{L-1} a_l x_{lp} e^{-j2\pi f_l(1+\beta_p)\tau} e^{j2\pi f_l \beta_p t} e^{j2\pi f_l t}\right\} + \tilde{e}(t)\end{aligned} \tag{6}$$

and hence the corresponding complex envelope at the output of the lth subchannel is

$$y_l(t) = a_l x_{lp} e^{-j2\pi f_l(1+\beta_p)\tau} e^{j2\pi f_l \beta_p t} + e_l(t). \tag{7}$$

Next, the information of the known range cell is incorporated into (7) by substituting $t = \tau + nT_{\mathrm{P}}, n = 0, 1, \ldots, N-1$, where T_{P} is the pulse repetition interval (PRI) and N is the number of temporal measurements within a given coherent processing interval (CPI). Hence, corresponding to a specific range cell containing the target, the complex envelope of the received signal at the output of the lth subchannel is

$$\begin{aligned} y_l(n) &= a_l x_{lp} \phi_l(n, p, \boldsymbol{v}) + e_l(n), \\ &\text{for } l = 0, 1, \ldots, L-1, \quad n = 0, 1, \ldots, N-1 \end{aligned} \tag{8}$$

where

$$\phi_l(n, p, \boldsymbol{v}) \triangleq e^{-j2\pi f_l \tau} e^{j2\pi f_l \beta_p n T_{\mathrm{P}}} \tag{9}$$

is a function of the unknown path index p through which the radar receives the information about the target, the unknown target-velocity $\boldsymbol{v}$, and the known target-delay τ.

B. Sparse Modeling

Suppose we discretize the possible signal paths and target velocities into P and V grid points, respectively. In general, the values of P and V could be very large. However, restricting our operation to a narrow region of interest (e.g., an urban canyon where the range is much greater than the width) and a few class of targets that have comparable velocities (e.g., cars/trucks within a city environment), we can restrict the values of P and V to smaller numbers. Then, considering all possible

combinations of $(p_i, \boldsymbol{v}_j), i = 1,2,\ldots,P, j = 1,2,\ldots,V$, we can rewrite (8) as

$$y_l(n) = a_l \boldsymbol{\phi}_l(n)^T \boldsymbol{x}_l + e_l(n) \tag{10}$$

where

- $\boldsymbol{\phi}_l(n) = [\phi_l(n, p_1, \boldsymbol{v}_1), \ldots, \phi_l(n, p_1, \boldsymbol{v}_V), \ldots, \phi_l(n, p_P, \boldsymbol{v}_V)]^T$;
- $\boldsymbol{x}_l$ is a $PV \times 1$ sparse-vector, having only k_l nonzero entries corresponding to the true signal paths and target velocity; i.e., [see (11), shown at the bottom of the page].

Stacking the measurements of all subchannels into an $L \times 1$ vector, we get

$$\boldsymbol{y}(n) = \boldsymbol{A}\boldsymbol{\Phi}(n)\boldsymbol{x} + \boldsymbol{e}(n), \tag{12}$$

where

- $\boldsymbol{y}(n) = [y_0(n), y_1(n), \ldots, y_{L-1}(n)]^T$;
- $\boldsymbol{A} = \mathrm{diag}(\boldsymbol{a})$ is an $L \times L$ complex diagonal matrix that contains the transmitted weights $\boldsymbol{a}$;
- $\boldsymbol{\Phi}(n) = \mathrm{blkdiag}(\boldsymbol{\phi}_0(n)^T, \boldsymbol{\phi}_2(n)^T, \ldots, \boldsymbol{\phi}_{L-1}(n)^T)$ is an $L \times LPV$ complex rectangular block-diagonal matrix;
- $\boldsymbol{x} = [\boldsymbol{x}_0^T, \boldsymbol{x}_1^T, \ldots, \boldsymbol{x}_{L-1}^T]^T$ is an $LPV \times 1$ sparse-vector that has $k = \sum_{l=0}^{L-1} k_l$ nonzero entries representing the scattering coefficients of the target along the received paths;
- $\boldsymbol{e}(n) = [e_0(n), e_1(n), \ldots, e_{L-1}(n)]^T$ is an $L \times 1$ vector of clutter returns, measurement noise, and co-channel interference.

Then, concatenating all the temporal data columnwise into an $LN \times 1$ vector, we obtain the OFDM measurement model as follows:

$$\boldsymbol{y} = \boldsymbol{\Phi}\boldsymbol{x} + \boldsymbol{e} \tag{13}$$

where

- $\boldsymbol{y} = [\boldsymbol{y}(0)^T, \boldsymbol{y}(1)^T, \ldots, \boldsymbol{y}(N-1)^T]^T$;
- $\boldsymbol{\Phi} = [(\boldsymbol{A}\boldsymbol{\Phi}(0))^T \ldots (\boldsymbol{A}\boldsymbol{\Phi}(N-1))^T]^T$ is an $LN \times LPV$ matrix containing all possible combinations of signal path and target velocity;
- $\boldsymbol{e} = [\boldsymbol{e}(0)^T, \boldsymbol{e}(1)^T, \ldots, \boldsymbol{e}(N-1)^T]^T$ is an $LN \times 1$ vector comprising clutter returns, noise, and interference.

C. Statistical Assumptions

In our problem, the clutter could be the contribution of undesired reflections from the environment surrounding or behind the target, or random multipath reflections from the irregularities on the reflecting surface (e.g., windows and balconies of the buildings in an urban scenario), that cannot be modeled as specular components. In (12), the noise vector $\boldsymbol{e}(n)$ models the clutter returns, measurement noise, and co-channel interference at the output of L subchannels. We assume that $\boldsymbol{e}(n)$ is a temporally white and circularly symmetric zero-mean complex Gaussian vector, correlated among different subchannels with positive definite covariance matrix $\boldsymbol{\Sigma}$. This assumption implies that the OFDM measurements in (13) are distributed as

$$\boldsymbol{y} \sim \mathbb{C}\mathcal{N}_{LN}(\boldsymbol{\Phi}\boldsymbol{x}, \boldsymbol{I}_N \otimes \boldsymbol{\Sigma}). \tag{14}$$

III. Sparse Recovery and Performance Analysis

In this section, we first develop a sparse recovery algorithm for the measurement model presented in the previous section. Then, we analytically evaluate its performance characteristics in terms of an upper bound on the ℓ_2-norm of the sparse-estimation error.

A. Sparse Recovery

In our measurement model (13), we have a sparse vector $\boldsymbol{x}$; i.e., $\boldsymbol{x}$ has only a few nonzero components. The sparsity level k of $\boldsymbol{x}$ is defined as the number of nonzero elements in $\boldsymbol{x}$, or in other words $k = \|\boldsymbol{x}\|_0$. The goal of the reconstruction algorithm is to estimate the vector $\boldsymbol{x}$ from the noisy measurement $\boldsymbol{y}$ by exploiting the sparsity. One of the most popular approaches of sparse signal recovery is the Dantzig selector. It belongs to the class of convex relaxation methods in which the ℓ_0 norm is replaced by the ℓ_1 norm that remains a measure of sparsity while being a convex function. The Dantzig selector provides an estimate of $\boldsymbol{x}$ as a solution to the following ℓ_1-regularization problem:

$$\min_{\boldsymbol{z} \in \mathbb{C}^{LPV}} \|\boldsymbol{z}\|_1 \text{ subject to } \|\boldsymbol{\Phi}^H(\boldsymbol{y} - \boldsymbol{\Phi}\boldsymbol{z})\|_\infty \leq \lambda \cdot \sigma \tag{15}$$

where $\lambda = \sqrt{2\log(LPV)}$ is a control parameter that ensures that the residual $(\boldsymbol{y} - \boldsymbol{\Phi}\boldsymbol{z})$ is within the noise level and $\sigma = \sqrt{\mathrm{tr}(\boldsymbol{\Sigma})/L}$.

However, from the construction of $\boldsymbol{x}$ in (10) and (12), we observe an additional structure, described as follows:

$$\boldsymbol{x} = \left[\boldsymbol{x}_0^T, \boldsymbol{x}_1^T, \ldots, \boldsymbol{x}_{L-1}^T\right]^T \tag{16}$$

where each $\boldsymbol{x}_l$, $l = 0,1,\ldots,L-1$, is sparse with sparsity level $k_l = \|\boldsymbol{x}_l\|_0$, and $k = \sum_{l=0}^{L-1} k_l$. Furthermore, the system matrix $\boldsymbol{\Phi}$ in (13) can also be expressed as

$$\boldsymbol{\Phi} = [\boldsymbol{\Phi}_0 \boldsymbol{\Phi}_1 \cdots \boldsymbol{\Phi}_{L-1}] \tag{17}$$

where each block-matrix of dimension $LN \times PV$, defined as

$$\boldsymbol{\Phi}_l = [\boldsymbol{0} \cdots \boldsymbol{0} \underbrace{a_l \boldsymbol{\phi}_l(0)}_{\text{index}=l} \boldsymbol{0} \cdots \boldsymbol{0} \underbrace{a_l \boldsymbol{\phi}_l(N-1)}_{\text{index}=l+(N-1)L} \boldsymbol{0} \ldots \boldsymbol{0}]^T \tag{18}$$

is orthogonal to any other block-matrix; i.e., $\boldsymbol{\Phi}_{l_1}^H \boldsymbol{\Phi}_{l_2} = \boldsymbol{0}$ for $l_1 \neq l_2$. Here $\boldsymbol{\phi}_l(\cdot)$ is the same as the one defined in relation to (10). Note also the difference in notation between $\boldsymbol{\Phi}_l$ (which is a columnwise block-matrix) and $\boldsymbol{\Phi}(n)$ (which is a rowwise block-matrix), defined in (12).

$$k_l = |\mathcal{I}_l|, \quad \text{where}$$
$$\mathcal{I}_l = \{\tilde{i} \in [1, P]: \text{ target information is received along the } p_{\tilde{i}}\text{-th path}\}. \tag{11}$$

To exploit this additional structure in the sparse-recovery algorithm, we propose a better reconstruction algorithm that solves a collection of L small Dantzig selectors:

$$\min_{\boldsymbol{z}_l \in \mathbb{C}^{PV}} \|\boldsymbol{z}_l\|_1 \quad \text{subject to } \left\|\boldsymbol{\Phi}_l^H(\boldsymbol{y}-\boldsymbol{\Phi}_l\boldsymbol{z}_l)\right\|_\infty \le \lambda_l \cdot \sigma \quad (19)$$

where $\lambda_l = \sqrt{2\log(PV)}$. We show in the next subsection that (19) has advantages over (15) both in terms of computation and performance, because more prior structures of the sparse vector are exploited.

B. Performance Analysis

Many functions of the system matrix $\boldsymbol{\Phi}$ have been proposed to analyze the performance of methods used to recover $\boldsymbol{x}$ from $\boldsymbol{y}$, the most popular measure being the restricted isometry constant (RIC). However, for an arbitrary given matrix, the computation of RIC is extremely difficult. Therefore, in [24] we proposed a new, easily computable measure, ℓ_1-constrained minimal singular value (ℓ_1-CMSV) of $\boldsymbol{\Phi}$, to assess the reconstruction performance of an ℓ_1-based algorithm. According to [24, Def. 4], we define the ℓ_1-CMSV of $\boldsymbol{\Phi}$ as

$$\rho_s(\boldsymbol{\Phi}) = \min_{\boldsymbol{x}\neq\boldsymbol{0}, s_1(\boldsymbol{x})\le s} \frac{\|\boldsymbol{\Phi}\boldsymbol{x}\|_2}{\|\boldsymbol{x}\|_2}, \quad \text{for any } s \in [1, LPV] \quad (20)$$

and

$$s_1(\boldsymbol{x}) \triangleq \frac{\|\boldsymbol{x}\|_1^2}{\|\boldsymbol{x}\|_2^2} \le k, \quad \text{when} \quad k = \|\boldsymbol{x}\|_0. \quad (21)$$

Then, the performance of our decomposed DS in (19) is given by the following theorem.

Theorem 1: Suppose $\boldsymbol{x} \in \mathbb{C}^{LPV}$ is a k-sparse vector having an additional structure as presented in (16), with each $\boldsymbol{x}_l \in \mathbb{C}^{PV}$ being a k_l-sparse vector, and (13) is the measurement model. Choose $\lambda_l = \sqrt{2\log(PV)}$ in (19). Then, with high probability, $\hat{\boldsymbol{x}}$ satisfies

$$\|\hat{\boldsymbol{x}} - \boldsymbol{x}\|_2 \le 4\sqrt{\sum_{l=0}^{L-1} \frac{\lambda_l^2 k_l \sigma^2}{\rho_{4k_l}^4(\boldsymbol{\Phi}_l)}} \quad (22)$$

where the concentrated solution $\hat{\boldsymbol{x}} = [\hat{\boldsymbol{x}}_0^T, \hat{\boldsymbol{x}}_1^T, \ldots, \hat{\boldsymbol{x}}_{L-1}^T]^T$ is obtained by using the individual solutions, $\hat{\boldsymbol{x}}_l$, of (19). More specifically, if $\lambda_l = \sqrt{2(1+q)\log(PV)}$ for each $q \ge 0$ is used in (19), then the bound holds with probability greater than $1 - L(\sqrt{\pi(1+q)\log(PV)} \cdot (PV)^q)^{-1}$.

Proof: Let us define the unobserved measurements $\boldsymbol{y}_l = \boldsymbol{\Phi}_l\boldsymbol{x}_l + \boldsymbol{e}$. Note that due to the orthogonality of $\boldsymbol{\Phi}_l$s,

$$\begin{aligned}\boldsymbol{\Phi}_l^H(\boldsymbol{y}-\boldsymbol{\Phi}_l\boldsymbol{z}_l) &= \boldsymbol{\Phi}_l^H\left(\sum_{l'=0}^{L-1}\boldsymbol{\Phi}_{l'}\boldsymbol{x}_{l'} + \boldsymbol{e} - \boldsymbol{\Phi}_l\boldsymbol{z}_l\right)\\ &= \boldsymbol{\Phi}_l^T(\boldsymbol{\Phi}_l\boldsymbol{x}_l + \boldsymbol{e} - \boldsymbol{\Phi}_l\boldsymbol{z}_l)\\ &= \boldsymbol{\Phi}_l^T(\boldsymbol{y}_l - \boldsymbol{\Phi}_l\boldsymbol{z}_l). \end{aligned} \quad (23)$$

As a consequence, the L small Dantzig selectors in (19) are equivalent with

$$\min_{\boldsymbol{z}_l \in \mathbb{C}^{PV}} \|\boldsymbol{z}_l\|_1 \quad \text{subject to } \left\|\boldsymbol{\Phi}_l^H(\boldsymbol{y}_l-\boldsymbol{\Phi}_l\boldsymbol{z}_l)\right\|_\infty \le \lambda_l \cdot \sigma. \quad (24)$$

Then, denoting the individual solutions of (19) as $\hat{\boldsymbol{x}}_l$ and assuming $\|\boldsymbol{\Phi}_l^H\boldsymbol{e}\|_\infty \le \lambda_l$, from [24, Th. 2] we have

$$\|\hat{\boldsymbol{x}}_l - \boldsymbol{x}_l\|_2 \le 4\frac{\lambda_l\sqrt{k_l}\sigma}{\rho_{4k_l}^2(\boldsymbol{\Phi}_l)}. \quad (25)$$

Hence, defining the concatenated estimate as $\hat{\boldsymbol{x}} = [\hat{\boldsymbol{x}}_0^T, \hat{\boldsymbol{x}}_1^T, \ldots, \hat{\boldsymbol{x}}_{L-1}^T]^T$, we get

$$\|\hat{\boldsymbol{x}} - \boldsymbol{x}\|_2 = \sqrt{\sum_{l=0}^{L-1}\|\hat{\boldsymbol{x}}_l - \boldsymbol{x}_l\|_2^2} \le 4\sqrt{\sum_{l=0}^{L-1}\frac{\lambda_l^2 k_l\sigma^2}{\rho_{4k_l}^4(\boldsymbol{\Phi}_l)}}. \quad (26)$$

■

On the contrary, if we use the original DS in (15) to obtain an estimate $\hat{\boldsymbol{x}}_{\mathrm{DS}}$, then using [24, Th. 2], we get

$$\|\hat{\boldsymbol{x}}_{\mathrm{DS}} - \boldsymbol{x}\|_2 \le 4\frac{\lambda\sqrt{k}\sigma}{\rho_{4k}^2(\boldsymbol{\Phi})} \quad (27)$$

where $k = \sum_{l=0}^{L-1} k_l$ and $\|\boldsymbol{\Phi}^H\boldsymbol{e}\|_\infty \le \lambda = \sqrt{2\log(LPV)}$. We now have the following theorem:

Theorem 2: The collection of L small Dantzig selectors in (19) performs better than the original Dantzig selector in (15) as it has a smaller upper bound on the ℓ_2-norm of the sparse-estimation error:

$$4\sqrt{\sum_{l=0}^{L-1}\frac{\lambda_l^2 k_l\sigma^2}{\rho_{4k_l}^4(\boldsymbol{\Phi}_l)}} \le 4\frac{\lambda\sqrt{k}\sigma}{\rho_{4k}^2(\boldsymbol{\Phi})}. \quad (28)$$

Proof: See Appendix A. ■

IV. Adaptive Waveform Design

In this section, we develop an adaptive waveform design technique, based on a multiobjective optimization (MOO) approach, to improve the detection and estimation performance. From the discussion of the previous section it follows that we can adaptively design the signal parameters, a_l, to minimize the upper bound on the estimation error. Note here that the upper bound on the sparse-estimation error depends solely on the properties of the system matrix $\boldsymbol{\Phi}$. However, to achieve better performance it is also essential that the signal parameters adapt to the operational scenario involving dynamic target states and nonstationary environmental conditions. Hence, in addition to minimizing the upper bound on the estimation error, we propose maximizing another utility function based on the squared Mahalanobis-distance, which depends on the target and noise parameters ($\boldsymbol{x}$ and $\boldsymbol{\Sigma}$). In the following, we first describe these

two single-objective optimization problems and their respective solutions. Then, we discuss the multiobjective optimization method.

A. Minimizing the Error Bound

From (17), we first notice that each $\boldsymbol{\Phi}_l$ can be written as $\boldsymbol{\Phi}_l = a_l\tilde{\boldsymbol{\Phi}}_l$, and therefore we have $\rho^4_{4k_l}(\boldsymbol{\Phi}_l) = a_l^4\rho^4_{4k_l}(\tilde{\boldsymbol{\Phi}}_l)$. Then, to minimize the upper bound on the sparse-estimation error, we construct an optimization problem as

$$\boldsymbol{a}^{(1)} = \arg\min_{\boldsymbol{a}\in\mathbb{C}^L} \sum_{l=0}^{L-1} \frac{\lambda_l^2 k_l \sigma^2}{a_l^4 \rho^4_{4k_l}(\tilde{\boldsymbol{\Phi}}_l)} \text{ subject to } \boldsymbol{a}^H\boldsymbol{a} = 1. \tag{29}$$

Using the Lagrange-multiplier approach, we can easily obtain the solution of (29) as

$$a_l^{(1)} = \sqrt{\frac{(2\alpha_l)^{1/3}}{\sum_{l=0}^{L-1}(2\alpha_l)^{1/3}}}, \quad \text{for } l = 0, 1, \ldots, L-1 \tag{30}$$

where $\alpha_l = (\lambda_l^2 k_l \sigma^2)/(\rho^4_{4k_l}(\tilde{\boldsymbol{\Phi}}_l))$. However, the computation of $\rho_{4k_l}(\tilde{\boldsymbol{\Phi}}_l)$ is difficult with the complex variables. Therefore, we use a computable lower bound on $\rho_{4k_l}(\tilde{\boldsymbol{\Phi}}_l)$, defined as

$$\rho_{8k_l}(\tilde{\boldsymbol{\Psi}}) \le \rho_{4k_l}(\tilde{\boldsymbol{\Phi}}_l) \tag{31}$$

where

$$\tilde{\boldsymbol{\Psi}}^T\tilde{\boldsymbol{\Psi}} = \begin{bmatrix} \boldsymbol{\Psi}_1^T\boldsymbol{\Psi}_1 + \boldsymbol{\Psi}_2^T\boldsymbol{\Psi}_2 & \boldsymbol{0} \\ \boldsymbol{0} & \boldsymbol{\Psi}_1^T\boldsymbol{\Psi}_1 + \boldsymbol{\Psi}_2^T\boldsymbol{\Psi}_2 \end{bmatrix},$$
$$\boldsymbol{\Psi}_1 = \operatorname{Re}\tilde{\boldsymbol{\Phi}}_{\boldsymbol{l}}, \quad \boldsymbol{\Psi}_2 = \operatorname{Im}\tilde{\boldsymbol{\Phi}}_{\boldsymbol{l}}. \tag{32}$$

See Appendix B for the details of (31). Then, similar to (30), we can obtain the optimal OFDM weights as

$$a_l^{(1)} = \sqrt{\frac{(2\tilde{\alpha}_l)^{1/3}}{\sum_{l=0}^{L-1}(2\tilde{\alpha}_l)^{1/3}}}, \quad \text{for} \quad l = 0, 1, \ldots, L-1 \tag{33}$$

where $\tilde{\alpha}_l = (\lambda_l^2 k_l \sigma^2)/(\rho^4_{8k_l}(\tilde{\boldsymbol{\Psi}}))$.

B. Maximizing the Mahalanobis-Distance

To decide whether a target is present or not in the range cell under test, the standard procedure is to construct a decision problem to choose between two possible hypotheses: the null hypothesis $\mathcal{H}_0$ (target-free hypothesis) or the alternate hypothesis $\mathcal{H}_1$ (target-present hypothesis). The problem can be expressed as

$$\begin{cases} \mathcal{H}_0: & \boldsymbol{y} = \boldsymbol{e} \\ \mathcal{H}_1: & \boldsymbol{y} = \boldsymbol{\Phi x} + \boldsymbol{e}. \end{cases} \tag{34}$$

Hence, the measurement $\boldsymbol{y}$ is distributed as either $\mathbb{CN}_{LN}(\boldsymbol{0}, \boldsymbol{I}_N \otimes \boldsymbol{\Sigma})$ or $\mathbb{CN}_{LN}(\boldsymbol{\Phi x}, \boldsymbol{I}_N \otimes \boldsymbol{\Sigma})$. To distinguish between these two distributions, one standard measure is the squared Mahalanobis-distance, defined as

$$d^2 = \boldsymbol{x}^H\boldsymbol{\Phi}^H(\boldsymbol{I}_N \otimes \boldsymbol{\Sigma})^{-1}\boldsymbol{\Phi x},$$
$$= \sum_{n=0}^{N-1} \boldsymbol{x}^H\boldsymbol{\Phi}(n)^H\boldsymbol{A}^H\boldsymbol{\Sigma}^{-1}\boldsymbol{A}\boldsymbol{\Phi}(n)\boldsymbol{x}. \tag{35}$$

Then, to maximize the detection performance, we can formulate an optimization problem as

$$\boldsymbol{a}^{(2)} = \arg\max_{\boldsymbol{a}\in\mathbb{C}^L} \left[\sum_{n=0}^{N-1} \boldsymbol{x}^H\boldsymbol{\Phi}(n)^H\boldsymbol{A}^H\boldsymbol{\Sigma}^{-1}\boldsymbol{A}\boldsymbol{\Phi}(n)\boldsymbol{x}\right], \quad \text{subject to } \boldsymbol{a}^H\boldsymbol{a} = 1. \tag{36}$$

After some algebraic manipulations (see Appendix C for details) we can rewrite this problem as

$$\boldsymbol{a}^{(2)} = \arg\max_{\boldsymbol{a}\in\mathbb{C}^L} \boldsymbol{a}^H \left[\sum_{n=0}^{N-1} (\boldsymbol{\Phi}(n)\boldsymbol{x}\boldsymbol{x}^H\boldsymbol{\Phi}(n)^H)^T \odot \boldsymbol{\Sigma}^{-1}\right]\boldsymbol{a}, \quad \text{subject to } \boldsymbol{a}^H\boldsymbol{a} = 1. \tag{37}$$

Hence, the optimization problem reduces to a simple eigenvalue–eigenvector problem, and the solution of (37) is the eigenvector corresponding to the largest eigenvalue of $[\sum_{n=0}^{N-1}(\boldsymbol{\Phi}(n)\boldsymbol{x}\boldsymbol{x}^H\boldsymbol{\Phi}(n)^H)^T \odot \boldsymbol{\Sigma}^{-1}]$.

C. Multi-Objective Optimization

From the discussions of previous subsections we notice that if the solution of (33) is used one would achieve an efficient sparse-estimation result. Alternatively, solving (37) we might get improved performance of the underlying detection problem. Hence, based on these arguments, we devise a constrained MOO problem to design the spectral parameters of the OFDM waveform, a_l, such that the upper bound on the sparse-estimation error is minimized and the squared Mahalanobis-distance of the detection problem is simultaneously maximized. Mathematically, this is represented as (38), shown at the bottom of the page. We employ the standard nondominated sorting genetic algorithm II (NSGA-II) [35] to solve our MOO problem, imposing a restriction on the solutions to satisfy the constraint $\boldsymbol{a}^H\boldsymbol{a} = 1$. The use of NSGA-II provides us with multiple Pareto-optimal solutions in a single run.

V. Numerical Results

In this section, we present the results of several numerical examples to illustrate the sparse-estimation performance for a

$$\boldsymbol{a}_{\text{opt}} = \begin{cases} \arg\min_{\boldsymbol{a}\in\mathbb{C}^L} \sum_{l=0}^{L-1} \frac{\lambda_l^2 k_l \sigma^2}{a_l^4 \rho^4_{4k_l}(\tilde{\boldsymbol{\Phi}}_l)}, \\ \arg\max_{\boldsymbol{a}\in\mathbb{C}^L} \boldsymbol{a}^H \left[\sum_{n=0}^{N-1} (\boldsymbol{\Phi}(n)\boldsymbol{x}\boldsymbol{x}^H\boldsymbol{\Phi}(n)^H\Big)^T \odot \boldsymbol{\Sigma}^{-1}\right]\boldsymbol{a} \end{cases} \quad \text{subject to } \boldsymbol{a}^H\boldsymbol{a} = 1. \tag{38}$$

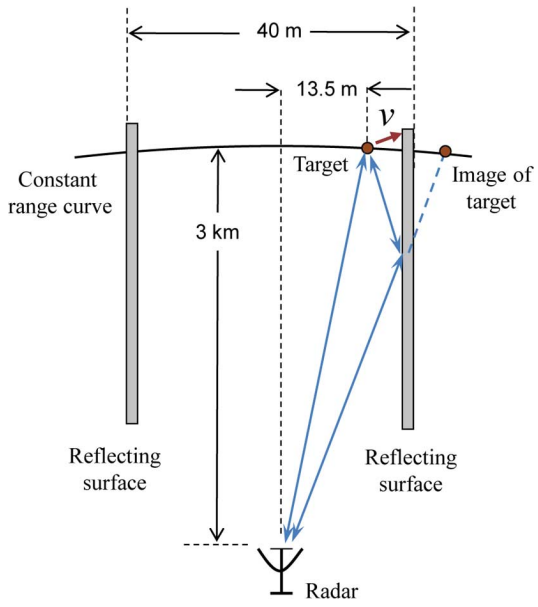

Fig. 2. A schematic representation of the multipath scenario considered in the numerical examples.

target-detection problem and to demonstrate the performance improvement due to the adaptive OFDM waveform design technique. First, we provide a description of the simulation setup and then discuss different numerical examples.

Fig. 2 schematically describes a scenario that we used in the simulations. For simplicity we considered a 2-D scenario, where both the radar and target were in the same plane. Our analyses can easily be extended to 3-D scenarios. The details of the target and radar parameters are as follows.

- Target and multipath parameters:
  - — Throughout a given CPI, the target remained within a particular range cell. We simulated the situation of a range cell that is at a distance of 3 km from the radar (positioned at the origin).
  - — The target was 13.5 m east from the center line, moving with velocity $\boldsymbol{v} = (35/\sqrt{2})(\hat{i} + \hat{j})$ m/s.
  - — There were two different paths between the target and radar: one direct and one reflected, subtending angles of 0.26° and 0.51°, respectively, with respect to the radar.
- Radar parameters:
  - — Carrier frequency $f_c = 1$ GHz.
  - — Available bandwidth $B = 100$ MHz.
  - — Number of OFDM subcarriers $L = 3$.
  - — Subcarrier spacing of $\Delta f = B/(L+1) = 25$ MHz.
  - — Pulsewidth $T = 1/\Delta f = 40$ ns.
  - — Pulse repetition interval $T_P = 4$ ms.
  - — Number of coherent pulses $N = 20$.
  - — All the transmit OFDM weights were equal; i.e., $a_l = 1/\sqrt{L} \quad \forall \quad l$.

To apply a sparse estimation approach, we partitioned the signal paths and target velocities into $P = 5$ and $V = 3$ uniform grid points. We considered signal paths that subtended angles of $\{-0.5^\circ, -0.25^\circ, 0^\circ, 0.25^\circ, 0.5^\circ\}$ with respect to the radar and target velocities of $\{25, 35, 45\}$ m/s. Hence, according to our description in Section II-B, we had $k_l = 2 \quad \forall\, l$ and $k = 6$. We generated the noise samples from a $\mathbb{CN}(0,1)$ distribution, and then scaled the samples to satisfy the required target to clutter-plus-noise ratio (TCNR), defined as

$$\mathrm{TCNR} = \frac{\boldsymbol{x}^H \boldsymbol{x}}{NL\sigma_0^2}. \tag{39}$$

Here we kept the clutter-plus-noise power the same across all the subcarriers by considering $\boldsymbol{\Sigma} = \sigma_0^2 \boldsymbol{I}_L$. The scattering coefficients of the target, $\boldsymbol{x}$, were varied to simulate different operational scenarios, the details of which are described later.

We analyzed the performance characteristics of our proposed technique in terms of the following two measures.

1) Root mean-square error (RMSE): Since we applied a sparse estimation approach, the standard performance measure is given by the RMSE of the estimated vector with respect to the true sparse vector, i.e., $||\hat{\boldsymbol{x}} - \boldsymbol{x}||_2$. We performed Monte Carlo simulations of 100 independent trials and averaged the results to obtain the RMSE values.
2) Empirical receiver operating characteristic (ROC): Since the underlying task was a target-detection problem, we also computed an empirical ROC to characterize our method. In our simulations, out of the total $LPV = 45$ grid points, $k = 6$ grid points contained the target responses, and the remaining $(LPV - k) = 39$ grid points did not have target responses. After each Monte Carlo run, we noted the number of grid points, n_T, that correspond to the estimated target response. Out of these n_T grid points, if n_D grid points lie within the set of true 6 grid points and if $n_{FA} = (n_T - n_D)$ lie within the remaining 39 grid points, then we can define the empirical probabilities of false alarm (P_{FA}) and detection (P_D) as

$$P_{FA} = \frac{n_{FA}}{LPV - k}, \quad P_D = \frac{n_D}{k}. \tag{40}$$

Finally, we averaged the results over 100 independent Monte Carlo runs to plot the empirical ROC.

A. Estimation and Detection Performance

We considered two different scenarios in our simulations. In Scenario 1, the target had equal scattering responses across all the subcarriers; i.e., $x_{l,d}^{(1)} = [1,1,1]^T$ and $x_{l,r}^{(1)} = [0.5, 0.5, 0.5]^T$ were the scattering coefficients in Scenario 1 along the direct and reflected paths, respectively. For Scenario 2 we considered varying target-responses over different subcarriers; i.e., $x_{l,d}^{(2)} = [4,1,2]^T$ and $x_{l,r}^{(2)} = [2, 0.5, 2]^T$. Figs. 3 and 4 show the performance characteristics of Scenario 1 and Scenario 2, respectively, at different TCNR values. We employed both the standard DS of (15) and our proposed decomposed DS of (19) to reconstruct the sparse vector. We notice that the decomposed DS performs better than the standard DS both in terms of normalized RMSE and empirical ROC, although the improvement is not huge apart from the low TCNR conditions. However, we get a drastic reduction in computation time (less than half of that required by the standard DS) when we used the decomposed DS.

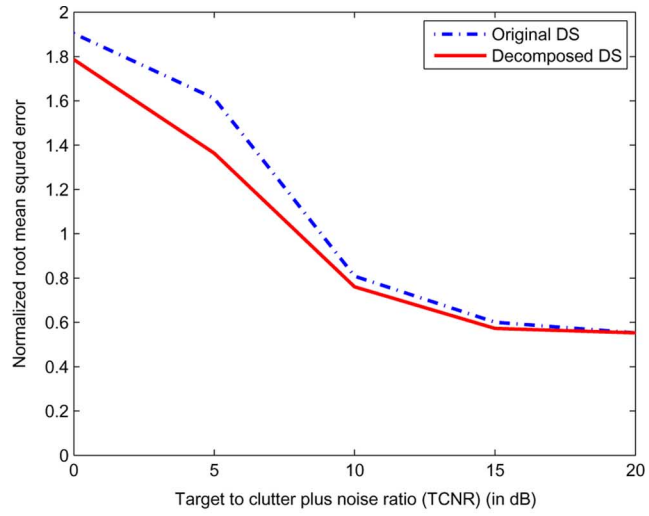

(a)

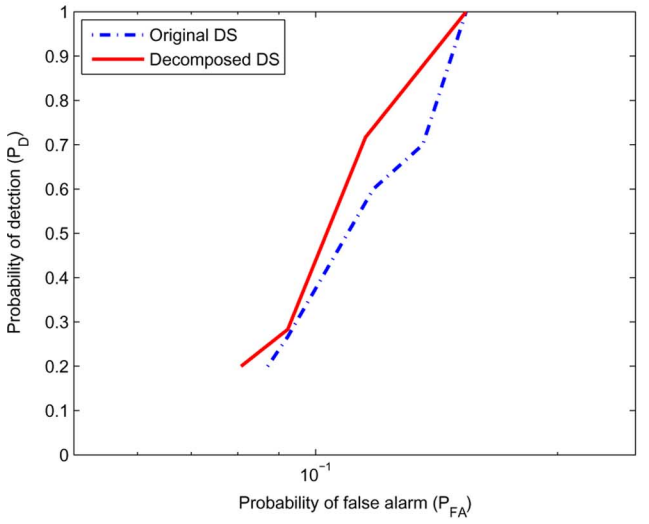

(b)

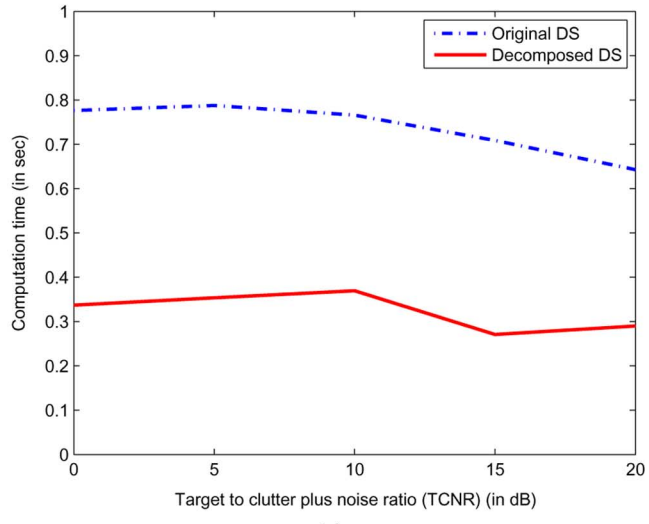

(c)

Fig. 3. Comparison of performances of the standard Dantzig selector and decomposed Dantzig selector in Scenario 1 in terms of the (a) normalized RMSE, (b) empirical ROC, and (c) computation time with respect to the target to clutter-plus-noise ratio.

B. Adaptive Waveform Design

To study the improvement in performance due to the adaptive waveform design techniques, we separately considered both the single-objective optimization problems in (33) and (37) and the multiobjective optimization method in (38) for two different scenarios.

Minimizing the upper bound on the sparse-estimation error, i.e., as a solution of (33), yielded $\boldsymbol{a}^{(1)} = [0.54, 0.16, 0.83]$. This solution depends only on the properties of the system matrix $\boldsymbol{\Phi}$. It implies that we can expect improved performance due to the use of this $\boldsymbol{a}^{(1)}$ irrespective of the target and noise parameters, which is evident from Figs. 7 and 8 for Scenarios 1 and 2, respectively.

In (37), the matrix $[\sum_{n=0}^{N-1}(\boldsymbol{\Phi}(n)\boldsymbol{x}\boldsymbol{x}^H\boldsymbol{\Phi}(n)^H)^T \odot \boldsymbol{\Sigma}^{-1}]$ became diagonal due to the choice of $\boldsymbol{\Sigma} = \sigma_0^2\boldsymbol{I}_L$. Therefore, the eigenvector corresponding to the largest eigenvalue had only one entry equal to 1 with all others 0. For example, in Scenario 1 all the diagonal entries were equal, and so the solution of (37) could be either $\boldsymbol{a}^{(2)} = [1,0,0]^T$ or $[0,1,0]^T$ or $[0,0,1]^T$. In Scenario 2, which had a stronger reflection along the first subcarrier, the solution of (37) was $\boldsymbol{a}^{(2)} = [1,0,0]^T$. To check whether the solution of (37) puts all the transmitted energy along the subcarrier that has strongest target reflection energy, we devised Scenario 3 to have reflection coefficients $x_{l,\mathrm{d}}^{(3)} = [1,10,1]^T$ and $x_{l,\mathrm{r}}^{(3)} = [0.5,5,0.5]^T$, and found the optimal solution to be $\boldsymbol{a}^{(2)} = [0,1,0]^T$. Hence, we concluded that the maximization of the Mahalanobis distance provided an adaptive waveform with all the signal energy transmitted over a single subcarrier that had the strongest target response. However, while doing so we were effectively using a single-carrier waveform that could not provide any frequency diversity. Therefore, we did not analyze the performance of our system with this type of adaptive waveform.

To solve the MOO problem (38), we employed the NSGA-II with the following parameters: population size $= 500$, number of generations $= 50$, crossover probability $= 0.9$, and mutation probability $= 0.1$. We applied the constraint $\boldsymbol{a}^H\boldsymbol{a} = 1$ in a relaxed way by ensuring that the solutions satisfy $0.999 \leq \boldsymbol{a}^H\boldsymbol{a} \leq 1.001$. We plotted the results of the optimal solutions and corresponding values of the two objective functions (at three different generations) in Figs. 5 and 6 for Scenarios 1 and 2, respectively. The constraint $\boldsymbol{a}^H\boldsymbol{a} = 1$ ensured that all the solutions could be represented on the surface of a sphere, restricted to the first octant, when $|a_{1_{\mathrm{opt}}}|$, $|a_{2_{\mathrm{opt}}}|$, and $|a_{3_{\mathrm{opt}}}|$ constitute the axes in Cartesian coordinates. We further noticed that the solutions reach the optimal Pareto-front very quickly. By the end of the fifth generation almost all the solutions resided on or close to the Pareto-front. We took one of the solutions from the Pareto front after the fiftieth generation (e.g., $\boldsymbol{a}_{\mathrm{opt}} = [0.60, 0.40, 0.70]^T$ for Scenario 1 and $\boldsymbol{a}_{\mathrm{opt}} = [0.98, 0.11, 0.17]^T$ for Scenario 2) and evaluated the performance characteristics of our system. The results are shown in Figs. 7 and 8 for Scenarios 1 and 2, respectively. We observed that due to its dependence on the target parameters the NSGA-II optimized waveform, $\boldsymbol{a}_{\mathrm{opt}}$, performed better than both the ℓ_1-CMSV—based adaptive waveform, $\boldsymbol{a}^{(1)}$, and a fixed waveform having $a_l = 1/\sqrt{L} \quad \forall\, l$.

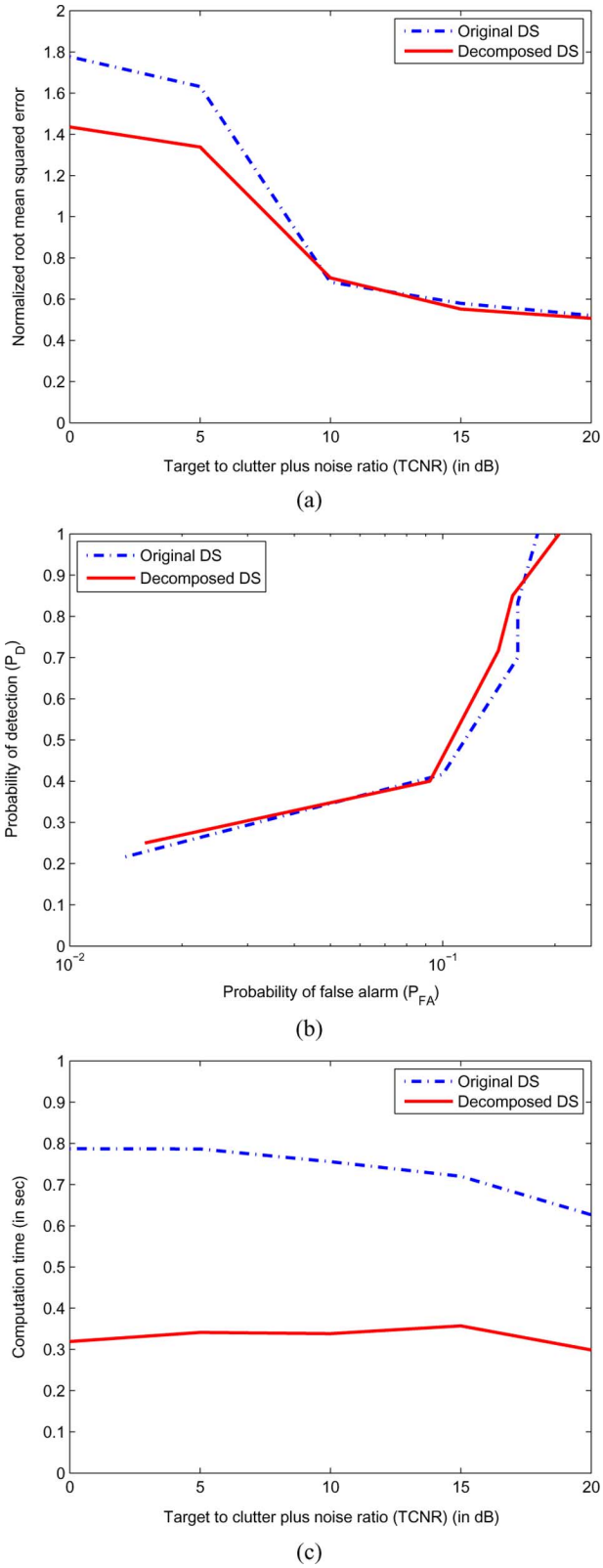

Fig. 4. Comparison of performances of the standard Dantzig selector and decomposed Dantzig selector in Scenario 2 in terms of the (a) normalized RMSE, (b) empirical ROC, and (c) computation time with respect to the target to clutter-plus-noise ratio.

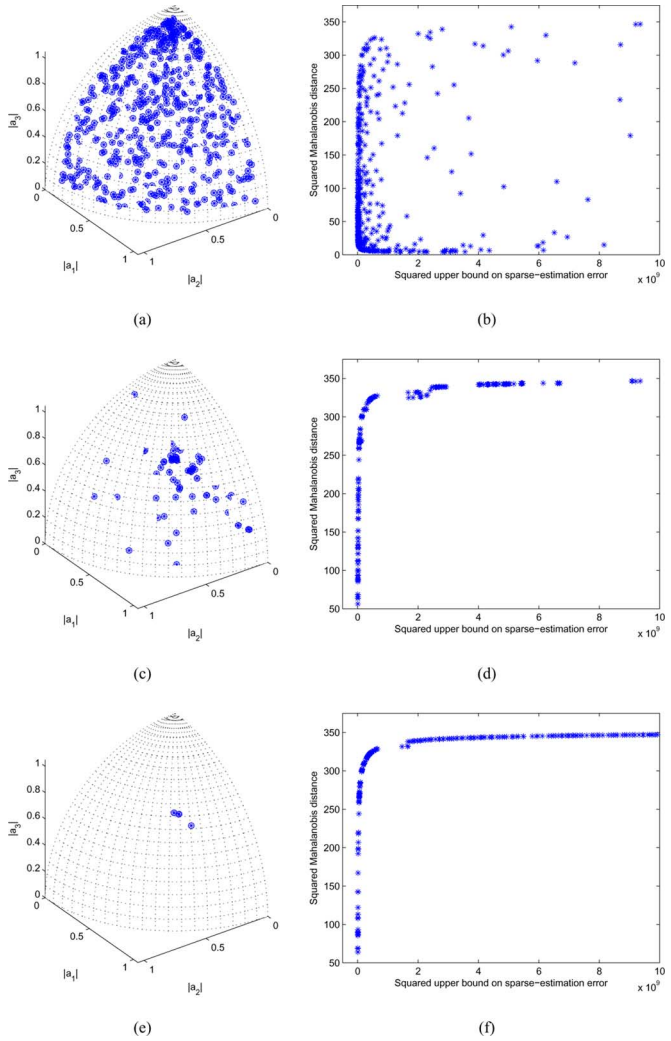

Fig. 5. Results of the NSGA-II in Scenario 1: (a), (b) optimal solutions and values of the objective functions at the zeroth generation; (c), (d) optimal solutions and values of the objective functions at the fifth generation; and (e), (f) optimal solutions and values of the objective functions at the fiftieth generation.

From the results of the MOO problem, we could also understand that there is some relationship between the energy-distributions of the optimal waveform, $\boldsymbol{a}_{\text{opt}}$, and that of the target response, $\boldsymbol{x}$, along different subcarriers. To investigate further, we took the average over the whole population of 500 solutions and found $\boldsymbol{a}_{\text{opt,avg}} = [0.61, 0.39, 0.68]^T$ in Scenario 1 and $\boldsymbol{a}_{\text{opt,avg}} = [0.88, 0.20, 0.36]^T$ in Scenario 2. Though it is not clear for Scenario 1, from the results of Scenario 2 we observed that the averaged distributions of energy of the optimal waveform across different subcarriers are in proportions to the distributions of target energy. As further confirmation, we ran the NSGA-II for Scenario 3 as well. Fig. 9 depicts the optimal solutions and corresponding values of the objective functions at the end of the fiftieth generation. In this case the average over all 500 solutions was $\boldsymbol{a}_{\text{opt,avg}} = [0.13, 0.96, 0.15]^T$. Hence, in general we can conclude that the solution of the MOO distributes the energy of the optimal waveform across different subcarriers in proportion to the distribution of the target energy; i.e., it puts more signal energy into that particular subcarrier in which the target response is stronger. Since in our simulation we kept the noise power fixed and varied the target energies over different subcarriers, we can extend our conclusion

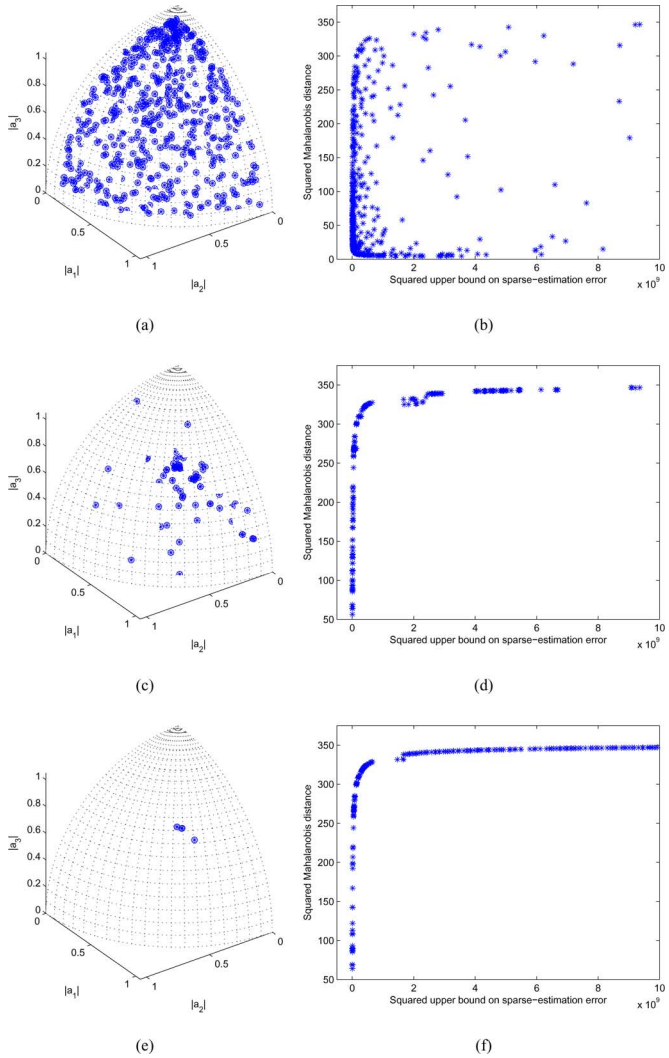

Fig. 6. Results of the NSGA-II in Scenario 2: (a), (b) optimal solutions and values of the objective functions at the zeroth generation; (c), (d) optimal solutions and values of the objective functions at the fifth generation; and (e), (f) optimal solutions and values of the objective functions at the fiftieth generation.

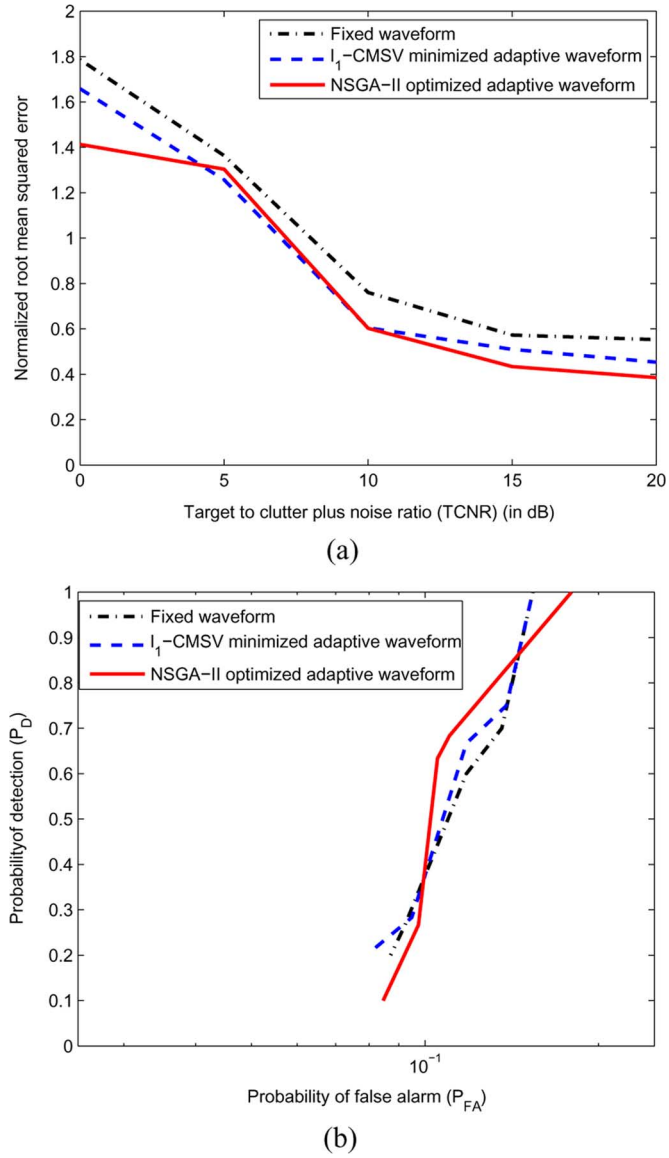

Fig. 7. Comparison of performances due to the fixed and adaptive waveforms in Scenario 1 in terms of the (a) normalized RMSE and (b) empirical ROC with respect to the target to clutter-plus-noise ratio.

by drawing synonymity between the target energy and TCNR value. In Fig. 10, we also demonstrated the performance of our system for Scenario 3 using fixed and adaptive waveforms.

VI. Conclusion

In this paper, we proposed a multiobjective optimization (MOO) technique to design the spectral parameters of an orthogonal-frequency-division multiplexing (OFDM) radar signal for detecting a moving target in the presence of multipath reflections. We first developed a parametric OFDM measurement model for a particular range cell under test, and then converted it to a sparse model that accounts for the target returns over all possible signal paths and target velocities. The use of an OFDM signal increased the frequency diversity of our system, as different scattering centers of a target resonate variably at different frequencies. In our model, the nonzero components of the sparse vector correspond to the scattering coefficients of the target at different OFDM subcarriers. To estimate the sparse vector, we employed a collection of multiple small Dantzig selectors (DS) that exploit more prior structures of the sparse vector. We also analytically evaluated the performance characteristics of our decomposed DS algorithm using the ℓ_1-constrained minimal singular value (ℓ_1-CMSV) of the measurement matrix and showed that it performs better than the standard DS algorithm. Furthermore, we proposed a criterion to optimally design the spectral parameters of the transmitting OFDM waveform for the next coherent processing interval, based on the MOO approach. We applied the nondominated sorting genetic algorithm II (NSGA-II) to solve a constrained MOO problem that simultaneously optimizes two objective functions: minimizing the upper bound on the estimation error to improve the efficiency of sparse-recovery and maximizing the squared Mahalanobis-distance to increase the performance of the underlying detection problem. We presented numerical examples to illustrate the performance characteristics of the sparse recovery and demonstrate the achieved performance

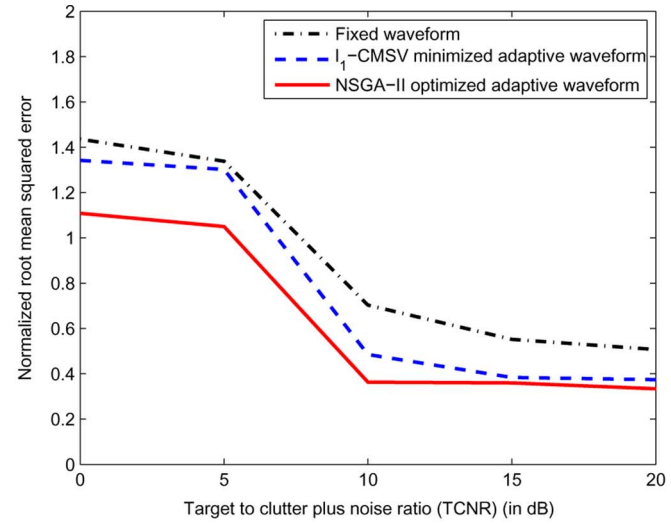

(a)

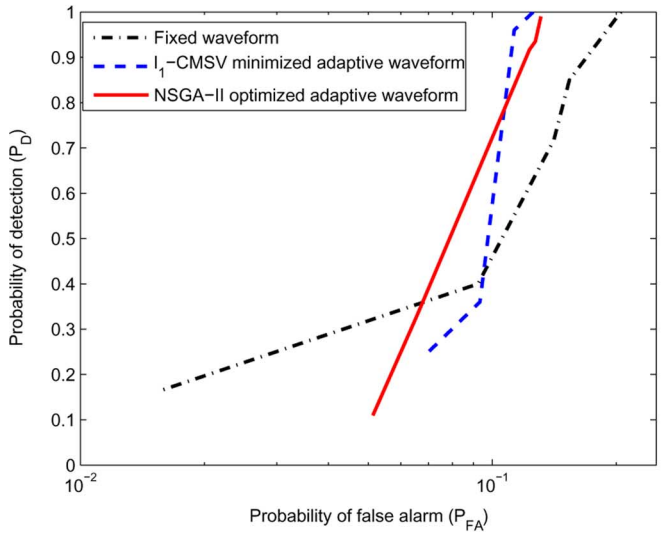

(b)

Fig. 8. Comparison of performances due to the fixed and adaptive waveforms in Scenario 2 in terms of the (a) normalized RMSE and (b) empirical ROC with respect to the target to clutter-plus-noise ratio.

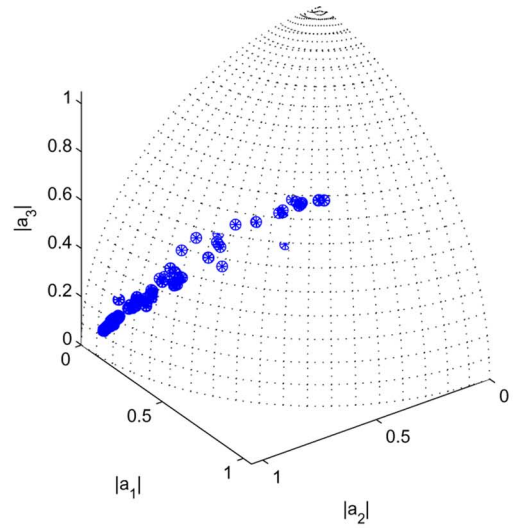

(a)

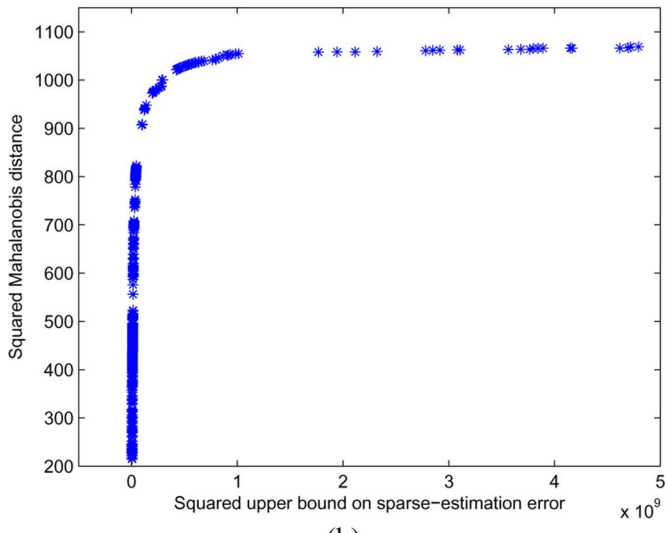

(b)

Fig. 9. Results of the NSGA-II in Scenario 3: (a), (b) optimal solutions and values of the objective functions at the fiftieth generation.

improvement due to adaptive OFDM waveform design. When the noise powers over different subcarriers were the same, we inferred that the solution of the MOO distributes the energy of the optimal waveform across different subcarriers in proportion to the distribution of the target energy.

In our future work, we will extend our model to incorporate more realistic physical effects, such as diffractions and refractions, which exist, for example, due to sharp edges and corners of the buildings or rooftops in an urban environment. We will incorporate other waveform design criteria, e.g., ambiguity function and similarity constraint, into the MOO algorithm. In addition, we will validate the performance of our proposed technique with real data.

APPENDIX A

In this Appendix, we provide a Proof of Theorem 2.

Consider vectors $\boldsymbol{z}_l \in \mathbb{C}^{PV}$ satisfying

$$s_1(\boldsymbol{z}_l) = \frac{||\boldsymbol{z}_l||_1^2}{||\boldsymbol{z}_l||_2^2} \leq 4k_l \tag{A1}$$

and a long vector $\boldsymbol{z} \in \mathbb{C}^{LPV}$ obtained after concatenating these $\boldsymbol{z}_l$s. Then, using the Cauchy–Schwartz inequality, we get

$$\begin{aligned} ||\boldsymbol{z}||_1 &= \sum_{l=0}^{L-1} ||\boldsymbol{z}_l||_1 \\ &\leq 2 \sum_{l=0}^{L-1} \sqrt{k_l} ||\boldsymbol{z}_l||_2 \\ &\leq 2 \sqrt{\sum_{l=0}^{L-1} k_l} \sqrt{\sum_{l=0}^{L-1} ||\boldsymbol{z}_l||_2^2} \\ &= 2\sqrt{k} ||\boldsymbol{z}||_2 \end{aligned}$$

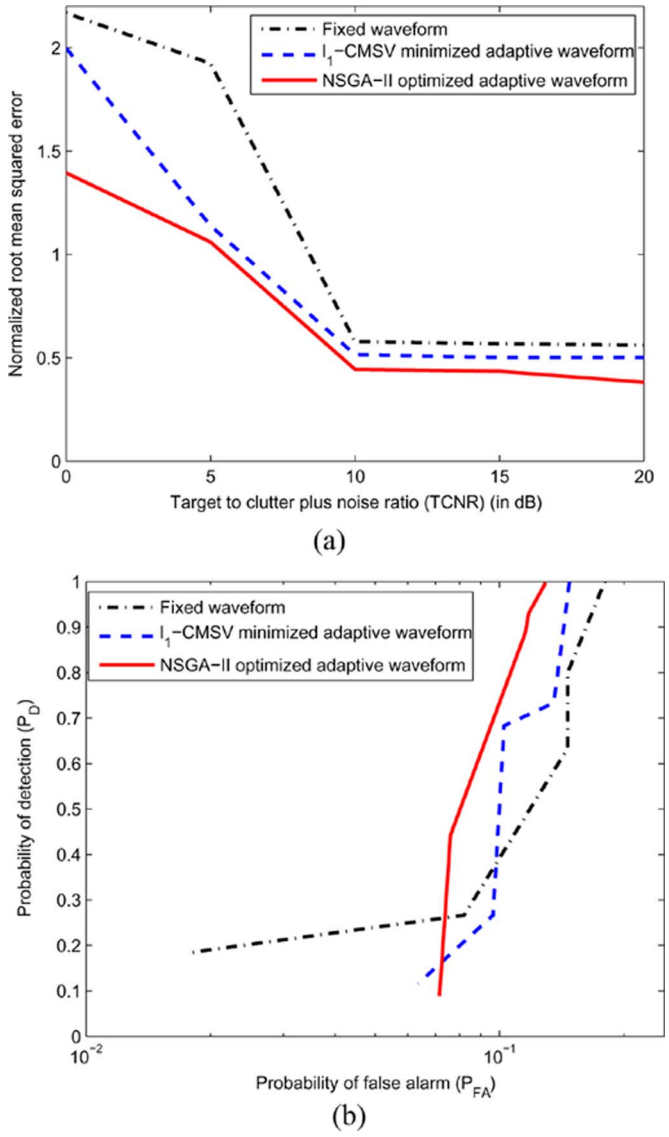

Fig. 10. Comparison of performances due to the fixed and adaptive waveforms in Scenario 3 in terms of the (a) normalized RMSE and (b) empirical ROC with respect to the target to clutter-plus-noise ratio.

that is,

$$s_1(\boldsymbol{z}) = \frac{\|\boldsymbol{z}\|_1^2}{\|\boldsymbol{z}\|_2^2} \le 4k. \tag{A2}$$

As a consequence, for any such constructed $\mathbf{z}$, we have

$$\rho_{4k}^2(\boldsymbol{\Phi}) \le \frac{z^H \boldsymbol{\Phi}^H \boldsymbol{\Phi} z}{z^H z} = \sum_{l=0}^{L-1} \frac{z_l^H \boldsymbol{\Phi}_l^H \boldsymbol{\Phi}_l z_l}{z^H z}.$$

Taking a $\mathbf{z_l}$ such that $\|z_l\|_2^2 = \omega_l \ge 0$ with $\|z\|_2^2 = \sum_{l=0}^{L-1} \omega_l = 1$, and

$$\omega_l \rho_{4k_l}^2(\boldsymbol{\Phi}_l) = z_l^H \boldsymbol{\Phi}_l^H \boldsymbol{\Phi}_l z_l,$$

we get

$$\rho_{4k}^2(\boldsymbol{\Phi}) \le \sum_{l=0}^{L-1} \omega_l \rho_{4k_l}^2(\boldsymbol{\Phi}_l). \tag{A3}$$

In particular, we have

$$\rho_{4k}^2(\boldsymbol{\Phi}) \le \rho_{4k_l}^2(\boldsymbol{\Phi}_l). \tag{A4}$$

Moreover, noticing that $\lambda_l \le \lambda$, we obtain

$$\sum_{l=0}^{L-1} \frac{\lambda_l^2 k_l \sigma^2}{\rho_{4k_l}^4(\boldsymbol{\Phi}_l)} \le \sum_{l=0}^{L-1} \frac{\lambda^2 k_l \sigma^2}{\rho_{4k}^4(\boldsymbol{\Phi})} = \frac{\lambda^2 k \sigma^2}{\rho_{4k}^4(\boldsymbol{\Phi})}. \tag{A5}$$

Appendix B

In this Appendix, we provide the details of the relationship presented in (31), i.e., how to obtain a computable lower bound on the original complex ℓ_1-CMSV.

In (30), $\rho_{4k_l}(\tilde{\boldsymbol{\Phi}}_l)$ corresponds to a solution of the following problem:

$$\min_{\boldsymbol{z}_l \in \mathbb{C}^{PV}} \boldsymbol{z}_l^H \tilde{\boldsymbol{\Phi}}_l^H \tilde{\boldsymbol{\Phi}}_l \boldsymbol{z}_l \text{ subject to } \|\boldsymbol{z}_l\|_1 \le \sqrt{4k_l}, \|\boldsymbol{z}_l\|_2 = 1. \tag{B1}$$

However, $\boldsymbol{z}_l$ being a complex vector, $\|\boldsymbol{z}_l\|_1 = \sum_{i=1}^{PV} \sqrt{(\mathrm{Re}\, z_{l,i})^2 + (\mathrm{Im}\, z_{l,i})^2}$ is not everywhere differentiable with respect to $\mathrm{Re}\ \boldsymbol{z}_l$ and $\mathrm{Im}\ \boldsymbol{z}_l$. Defining $\boldsymbol{g} = \mathrm{Re}\, \boldsymbol{z}_l, \boldsymbol{h} = \mathrm{Im}\, \boldsymbol{z}_l$, and $\boldsymbol{\Psi}_1 = \mathrm{Re}\tilde{\boldsymbol{\Phi}}_l$, $\boldsymbol{\Psi}_2 = \mathrm{Im}\tilde{\boldsymbol{\Phi}}_l$, we have

$$\begin{aligned} \boldsymbol{z}_l^H \tilde{\boldsymbol{\Phi}}_l^H \tilde{\boldsymbol{\Phi}}_l \boldsymbol{z}_l = \boldsymbol{g}^T \left(\boldsymbol{\Psi}_1^T \boldsymbol{\Psi}_1 + \boldsymbol{\Psi}_2^T \boldsymbol{\Psi}_2\right) \boldsymbol{g} \\ + \boldsymbol{h}^T \left(\boldsymbol{\Psi}_1^T \boldsymbol{\Psi}_1 + \boldsymbol{\Psi}_2^T \boldsymbol{\Psi}_2\right) \boldsymbol{h} \end{aligned} \tag{B2}$$

and note that

$$\begin{aligned} \|\boldsymbol{z}_l\|_1 &= \sum_{i=1}^{PV} \sqrt{g_i^2 + h_i^2} \\ &\ge \frac{\sqrt{2}}{2} \sum_{i=1}^{PV} (|g_i| + |h_i|) \\ &= \frac{1}{\sqrt{2}} \|[\boldsymbol{g}^T, \boldsymbol{h}^T]^T\|_1 \end{aligned} \tag{B3}$$

$$\|\boldsymbol{z}_l\|_2 = \sum_{i=1}^{PV} \left(g_i^2 + h_i^2\right) = \|[\boldsymbol{g}^T, \boldsymbol{h}^T]^T\|_2. \tag{B4}$$

Therefore, we can compute a lower bound on the original complex ℓ_1-CMSV as a solution of the following problem:

$$\begin{aligned} &\min_{\substack{\boldsymbol{g} \in \mathbb{R}^{PV} \\ \boldsymbol{h} \in \mathbb{R}^{PV}}} \begin{bmatrix} \boldsymbol{g}^T & \boldsymbol{h}^T \end{bmatrix} \\ &\quad \times \begin{bmatrix} \boldsymbol{\Psi}_1^T \boldsymbol{\Psi}_1 + \boldsymbol{\Psi}_2^T \boldsymbol{\Psi}_2 & \boldsymbol{0} \\ \boldsymbol{0} & \boldsymbol{\Psi}_1^T \boldsymbol{\Psi}_1 + \boldsymbol{\Psi}_2^T \boldsymbol{\Psi}_2 \end{bmatrix} \begin{bmatrix} \boldsymbol{g} \\ \boldsymbol{h} \end{bmatrix}, \\ &\text{subject to } \left\| \begin{bmatrix} \boldsymbol{g} \\ \boldsymbol{h} \end{bmatrix} \right\|_1 \le \sqrt{8k_l} \text{ and } \left\| \begin{bmatrix} \boldsymbol{g} \\ \boldsymbol{h} \end{bmatrix} \right\|_2 = 1. \end{aligned} \tag{B5}$$

Then, denoting the solution of (B5) as $\rho_{8k_l}(\tilde{\boldsymbol{\Psi}})$, where

$$\tilde{\boldsymbol{\Psi}}^T\tilde{\boldsymbol{\Psi}} = \begin{bmatrix} \boldsymbol{\Psi}_1^T\boldsymbol{\Psi}_1 + \boldsymbol{\Psi}_2^T\boldsymbol{\Psi}_2 & \mathbf{0} \\ \mathbf{0} & \boldsymbol{\Psi}_1^T\boldsymbol{\Psi}_1 + \boldsymbol{\Psi}_2^T\boldsymbol{\Psi}_2 \end{bmatrix}$$

we get

$$\rho_{8k_l}(\tilde{\boldsymbol{\Psi}}) \leq \rho_{4k_l}(\tilde{\boldsymbol{\Phi}}_l). \tag{B6}$$

APPENDIX C

In this Appendix, we show how we simplify the objective function in (36) to that in (37).

First, using the relationship between a trace and vec operator, $\mathrm{tr}(\boldsymbol{UV}) = \mathrm{vec}(\boldsymbol{U}^T)^T\mathrm{vec}(\boldsymbol{V})$, we get

$$\begin{aligned}
&\sum_{n=0}^{N-1} \boldsymbol{x}^H\boldsymbol{\Phi}(n)^H\boldsymbol{A}^H\boldsymbol{\Sigma}^{-1}\boldsymbol{A}\boldsymbol{\Phi}(n)\boldsymbol{x} \\
&\quad= \sum_{n=0}^{N-1} \mathrm{tr}(\boldsymbol{x}^H\boldsymbol{\Phi}(n)^H\boldsymbol{A}^H\boldsymbol{\Sigma}^{-1}\boldsymbol{A}\boldsymbol{\Phi}(n)\boldsymbol{x}), \\
&\quad= \sum_{n=0}^{N-1} \mathrm{tr}(\boldsymbol{A}^H\boldsymbol{\Sigma}^{-1}\boldsymbol{A}\boldsymbol{\Phi}(n)\boldsymbol{x}\boldsymbol{x}^H\boldsymbol{\Phi}(n)^H), \\
&\quad= \sum_{n=0}^{N-1} \mathrm{vec}((\boldsymbol{A}^H)^T)^T\mathrm{vec}(\boldsymbol{\Sigma}^{-1}\boldsymbol{A}\boldsymbol{\Phi}(n)\boldsymbol{x}\boldsymbol{x}^H\boldsymbol{\Phi}(n)^H).
\end{aligned} \tag{C1}$$

Then, we apply one of the properties of the vec operator, $\mathrm{vec}(\boldsymbol{UQV}) = (\boldsymbol{V}^T \otimes \boldsymbol{U})\mathrm{vec}(\boldsymbol{Q})$, to get

$$\begin{aligned}
&\mathrm{vec}((\boldsymbol{A}^H)^T)^T\mathrm{vec}(\boldsymbol{\Sigma}^{-1}\boldsymbol{A}\boldsymbol{\Phi}(n)\boldsymbol{x}\boldsymbol{x}^H\boldsymbol{\Phi}(n)^H) \\
&\quad= \mathrm{vec}((\boldsymbol{A}^H)^T)^T[(\boldsymbol{\Phi}(n)\boldsymbol{x}\boldsymbol{x}^H\boldsymbol{\Phi}(n)^H)^T \otimes \boldsymbol{\Sigma}^{-1}]\mathrm{vec}(\boldsymbol{A}).
\end{aligned} \tag{C2}$$

Note that in our problem $\boldsymbol{A} = \mathrm{diag}(\boldsymbol{a})$ is a diagonal matrix. Therefore, $\mathrm{vec}(\boldsymbol{A})$ can be written as

$$\mathrm{vec}(\boldsymbol{A}) = \begin{bmatrix} \boldsymbol{C}_1 \\ \boldsymbol{C}_2 \\ \vdots \\ \boldsymbol{C}_L \end{bmatrix} \boldsymbol{a} \tag{C3}$$

where $\boldsymbol{C_l}$ is an $L \times L$ matrix that has a 1 only at the (l,l)th position and zero elsewhere. Similarly, we have

$$\mathrm{vec}((\boldsymbol{A}^H)^T)^T = \mathrm{vec}((\boldsymbol{A}^H))^T = \boldsymbol{a}^H \begin{bmatrix} \boldsymbol{C}_1 \\ \boldsymbol{C}_2 \\ \vdots \\ \boldsymbol{C}_L \end{bmatrix}^T. \tag{C4}$$

Additionally, from [41, Th. 1] we have

$$\begin{aligned}
&\begin{bmatrix} \boldsymbol{C}_1 \\ \boldsymbol{C}_2 \\ \vdots \\ \boldsymbol{C}_L \end{bmatrix}^T [(\boldsymbol{\Phi}(n)\boldsymbol{x}\boldsymbol{x}^H\boldsymbol{\Phi}(n)^H)^T \otimes \boldsymbol{\Sigma}^{-1}] \begin{bmatrix} \boldsymbol{C}_1 \\ \boldsymbol{C}_2 \\ \vdots \\ \boldsymbol{C}_L \end{bmatrix} \\
&\qquad= (\boldsymbol{\Phi}(n)\boldsymbol{x}\boldsymbol{x}^H\boldsymbol{\Phi}(n)^H)^T \odot \boldsymbol{\Sigma}^{-1}.
\end{aligned} \tag{C5}$$

Finally, substituting the results of (C3)–(C5) into (C2), we get

$$\begin{aligned}
&\mathrm{vec}((\boldsymbol{A}^H)^T)^T[(\boldsymbol{\Phi}(n)\boldsymbol{x}\boldsymbol{x}^H\boldsymbol{\Phi}(n)^H)^T \otimes \boldsymbol{\Sigma}^{-1}]\mathrm{vec}(\boldsymbol{A}) \\
&\qquad= \boldsymbol{a}^H[(\boldsymbol{\Phi}(n)\boldsymbol{x}\boldsymbol{x}^H\boldsymbol{\Phi}(n)^H)^T \odot \boldsymbol{\Sigma}^{-1}]\boldsymbol{a}
\end{aligned}$$

and therefore from (C1) we have

$$\begin{aligned}
&\sum_{n=0}^{N-1} \boldsymbol{x}^H\boldsymbol{\Phi}(n)^H\boldsymbol{A}^H\boldsymbol{\Sigma}^{-1}\boldsymbol{A}\boldsymbol{\Phi}(n)\boldsymbol{x} \\
&\quad= \sum_{n=0}^{N-1} \boldsymbol{a}^H[(\boldsymbol{\Phi}(n)\boldsymbol{x}\boldsymbol{x}^H\boldsymbol{\Phi}(n)^H)^T \odot \boldsymbol{\Sigma}^{-1}]\boldsymbol{a}, \\
&\quad= \boldsymbol{a}^H\left[\sum_{n=0}^{N-1} (\boldsymbol{\Phi}(n)\boldsymbol{x}\boldsymbol{x}^H\boldsymbol{\Phi}(n)^H)^T \odot \boldsymbol{\Sigma}^{-1}\right]\boldsymbol{a}.
\end{aligned} \tag{C6}$$

REFERENCES

[1] S. Sen, M. Hurtado, and A. Nehorai, "Adaptive OFDM radar for detecting a moving target in urban scenarios," in *Proc. Int. Waveform Diversity Design (WDD) Conf.*, Orlando, FL, Feb. 8–13, 2009, pp. 268–272.

[2] S. Sen and A. Nehorai, "Adaptive OFDM radar for target detection in multipath scenarios," *IEEE Trans. Signal Process.*, vol. 59, no. 1, pp. 78–90, Jan. 2011.

[3] J. Durek, *Multipath Exploitation Radar Industry Day*. Herndon, VA: DARPA, Aug. 17, 2009 [Online]. Available: http://www.darpa.mil/STO/ Solicitations/BAA09-01/presentations/MER_Industry_Day.pdf

[4] J. L. Krolik, J. Farrell, and A. Steinhardt, "Exploiting multipath propagation for GMTI in urban environments," in *Proc. IEEE Conf. Radar*, 2006, pp. 65–68.

[5] D. K. Barton, "Low-angle radar tracking," *Proc. IEEE*, vol. 62, no. 6, pp. 687–704, Jun. 1974.

[6] W. D. White, "Low-angle radar tracking in the presence of multipath," *IEEE Trans. Aerosp. Electron. Syst.*, vol. AES-10, no. 6, pp. 835–852, Nov. 1974.

[7] A. V. Mrstik and P. G. Smith, "Multipath limitations on low-angle radar tracking," *IEEE Trans. Aerosp. Electron. Syst.*, vol. AES-14, no. 1, pp. 85–102, Jan. 1978.

[8] Y. Bar-Shalom, A. Kumar, W. D. Blair, and G. W. Groves, "Tracking low elevation targets in the presence of multipath propagation," *IEEE Trans. Aerosp. Electron. Syst.*, vol. 30, no. 3, pp. 973–979, Jul. 1994.

[9] J. K. Jao, "A matched array beamforming technique for low angle radar tracking in multipath," in *Proc. IEEE Nat. Radar Conf.*, Atlanta, GA, Mar. 29–31, 1994, pp. 171–176.

[10] M. Papazoglou and J. L. Krolik, "Electromagnetic matched-field processing for target height finding with over-the-horizon radar," in *Proc. IEEE Int. Conf. Acoustics, Speech, Signal Process. (ICASSP)*, Munich, Germany, Apr. 21–24, 1997, vol. 1, pp. 559–562.

[11] H. Tajima, S. Fukushima, and H. Yokoyama, "A consideration of multipath detection in navigation systems," *Electron. Commun. Jpn. (Part I: Commun.)*, vol. 85, no. 11, pp. 52–59, May 2002.

[12] R. J. Urick, *Principles of Underwater Sound for Engineers*. New York: McGraw-Hill, 1967.

[13] R. Moose and T. Dailey, "Adaptive underwater target tracking using passive multipath time-delay measurements," *IEEE Trans. Acoust., Speech, Signal Process.*, vol. 33, no. 4, pp. 778–787, Aug. 1985.

[14] A. Pandharipande, "Principles of OFDM," *IEEE Potentials*, vol. 21, no. 2, pp. 16–19, Apr. 2002.

[15] A. F. Molisch, *Wideband Wireless Digital Communications*. Upper Saddle River, NJ: Prentice-Hall PTR, 2001.

[16] B. L. Floch, R. Halbert-Lassalle, and D. Castelain, "Digital sound broadcasting to mobile receivers," *IEEE Trans. Consum. Electron.*, vol. 35, no. 3, pp. 493–503, Aug. 1989.

[17] G. E. A. Franken, H. Nikookar, and P. V. Genderen, "Doppler tolerance of OFDM-coded radar signals," in *Proc. Eur. Radar Conf.*, Manchester, U.K., Sep. 13–15, 2006, pp. 108–111.

[18] D. S. Garmatyuk, "Simulated imaging performance of UWB SAR based on OFDM," in *Proc. IEEE Int. Conf. Ultra-Wideband*, Sep. 2006, pp. 237–242.

[19] J. P. Stralka, "Applications of orthogonal frequency-division multiplexing (OFDM) to radar," Ph.D. dissertation, The Johns Hopkins Univ., Baltimore, MD, Mar. 2008.
[20] S. S. Chen, D. L. Donoho, and M. A. Saunders, "Atomic decomposition by basis pursuit," *SIAM J. Sci. Comput.*, vol. 20, no. 1, pp. 33–61, Aug. 1998.
[21] D. Malioutov, M. Çetin, and A. S. Willsky, "A sparse signal reconstruction perspective for source localization with sensor arrays," *IEEE Trans. Signal Process.*, vol. 53, no. 8, pp. 3010–3022, Aug. 2005.
[22] E. Candès and T. Tao, "The Dantzig selector: Statistical estimation when p is much larger than n," *Ann. Stat.*, vol. 35, no. 6, pp. 2313–2351, 2007.
[23] R. Tibshirani, "Regression shrinkage and selection via the lasso," *J. R. Stat. Soc. B, Methodol.*, vol. 58, no. 1, pp. 267–288, 1996.
[24] G. Tang and A. Nehorai, "The ℓ_1-constrained minimal singular value: A computable quantification of the stability of sparse signal reconstruction," *IEEE Trans. Inf. Theory* Apr. 2010 [Online]. Available: http://arxiv.org/abs/1004.4222v1, submitted for publication
[25] E. J. Candès and T. Tao, "Decoding by linear programming," *IEEE Trans. Inf. Theory*, vol. 51, no. 12, pp. 4203–4215, Dec. 2005.
[26] E. J. Candès, "The restricted isometry property and its implications for compressed sensing," *Comptes. Rendus. Mathematique*, vol. 346, no. 9–10, pp. 589–592, May 2008.
[27] K. Deb, *Multi-Objective Optimization Using Evolutionary Algorithms*, 1st ed. New York: Wiley, Jun. 2001.
[28] C. A. C. Coello, G. B. Lamont, and D. A. V. Veldhuizen, *Evolutionary Algorithms for Solving Multi-Objective Problems*, 2nd ed. New York: Springer, 2007.
[29] E. Zitzler, M. Laumanns, and S. Bleuler, "A tutorial on evolutionary multiobjective optimization," in *Metaheuristics for Multiobjective Optimisation*, ser. Lecture Notes in Economics and Mathematical Systems, X. Gandibleux, M. Sevaux, K. Sörensen, and V. T'kindt, Eds. Berlin, Germany: Springer, 2004, vol. 535, pp. 3–37.
[30] R. T. Marler and J. S. Arora, "Survey of multi-objective optimization methods for engineering," *Structural Multidisciplin. Optim.*, vol. 26, no. 6, pp. 369–395, Mar. 2004.
[31] P. C. Mahalanobis, "On the generalized distance in statistics," in *Proc. Nat. Inst. Sci. India*, 1936, vol. 2, pp. 49–55.
[32] T. W. Anderson, *An Introduction to Multivariate Statistical Analysis*, 3rd ed. Hoboken, NJ: Wiley, 2003.
[33] F. Y. Edgeworth, *Mathematical Physics: An Essay on the Application of Mathematics to the Moral Sciences*. London, U.K.: C. K. Paul, 1881.
[34] V. Pareto, *Cours D'Economie Politique, Volume I and II*. Lausanne, Switzerland: F. Rouge, 1896.
[35] K. Deb, A. Pratap, S. Agarwal, and T. Meyarivan, "A fast and elitist multiobjective genetic algorithm: NSGA-II," *IEEE Trans. Evol. Comput.*, vol. 6, no. 2, pp. 182–197, Apr. 2002.
[36] J. W. Enslin, "An evolutionary algorithm approach to simultaneous multimission radar waveform design," Master's thesis, Rochester Inst. of Technology, Rochester, NY, Aug. 2007.
[37] S. Mittal and K. Deb, "Three-dimensional offline path planning for UAVs using multiobjective evolutionary algorithms," in *Proc. IEEE Congr. Evol. Comput. (CEC)*, Singapore, Sep. 25–28, 2007, pp. 3195–3202.
[38] B. R. Secrest and G. B. Lamont, "Multiobjective tuning of a multitarget tracking algorithm using an evolutionary algorithm," in *Proc. IEEE Symp. Computational Intelligence in Multi-Criteria Decision-Making (MCDM)*, Nashville, TN, Mar. 30–Apr. 2, 2009, pp. 51–57.
[39] V. Baghel, G. Panda, P. Srihari, K. Rajarajeswari, and B. Majhi, "An efficient multi-objective pulse radar compression technique using RBF and NSGA-II," in *Proc. World Congr. Nature Biologically Inspired Computing (NaBIC)*, Coimbatore, India, Dec. 9–11, 2009, pp. 1291–1296.
[40] V. Baghel, "Multiobjective Optimization—New formulation and application to radar signal processing," Master's thesis, National Inst. of Technology, Rourkela, India, 2009.
[41] G. Visick, "A quantitative version of the observation that the Hadamard product is a principal submatrix of the Kronecker product," *Linear Algebra Appl.*, vol. 304, no. 1–3, pp. 45–68, Jan. 2000.

Satyabrata Sen (S'07–M'10) received the B.E. degree in electronics and telecommunication engineering from Jadavpur University, India, in 2002, the M.Tech. degree in electrical engineering (with specialization in communication and signal processing) from Indian Institute of Technology Bombay, India, in 2005, and the Ph.D. degree in electrical and systems engineering from Washington University in St. Louis, MO, in 2010.

His research interests are in the area of statistical signal processing, detection and estimation theory, and their applications in radar, communications, and sensor arrays.

Mr. Sen received the second place award in the student paper competition at the Fifth International Waveform Diversity & Design (WDD) Conference 2010.

Gongguo Tang (S'09–M'09) received the B.Sc. degree in mathematics from the Shandong University, China, in 2003 and the M.Sc. degree in system science from Chinese Academy of Sciences, China, in 2006.

Currently, he is working towards the Ph.D. degree with the Department of Electrical and Systems Engineering, Washington University in St. Louis, under the guidance of Dr. A. Nehorai. His research interests are in the area of sparse signal processing, matrix completion, statistical signal processing, detection and estimation, and their applications.

Arye Nehorai (S'80–M'83–SM'90–F'94) received the B.Sc. and M.Sc. degrees from the Technion, Haifa, Israel, and the Ph.D. degree from Stanford University, Stanford, CA.

Previously, he was a faculty member at Yale University and the University of Illinois at Chicago. He is currently the Eugene and Martha Lohman Professor and Chair of the Department of Electrical and Systems Engineering at Washington University in St. Louis (WUSTL). He serves as the Director of the Center for Sensor Signal and Information Processing at WUSTL.

Dr. Nehorai has served as Editor-in-Chief of the IEEE TRANSACTIONS ON SIGNAL PROCESSING from 2000 to 2002. From 2003 to 2005, he was Vice-President (Publications) of the IEEE Signal Processing Society (SPS), Chair of the Publications Board, and member of the Executive Committee of this Society. He was the Founding Editor of the special columns on Leadership Reflections in the *IEEE Signal Processing Magazine* from 2003 to 2006. received the 2006 IEEE SPS Technical Achievement Award and the 2010 IEEE SPS Meritorious Service Award. He was elected Distinguished Lecturer of the IEEE SPS for the term 2004 to 2005. He was corecipient of the IEEE SPS 1989 Senior Award for Best Paper coauthor of the 2003 Young Author Best Paper Award and corecipient of the 2004 Magazine Paper Award. In 2001, he was named University Scholar of the University of Illinois. He is the Principal Investigator of the Multidisciplinary University Research Initiative (MURI) project entitled Adaptive Waveform Diversity for Full Spectral Dominance. He has been a Fellow of the Royal Statistical Society since 1996.